



# Coupling framework (1.0) for the PISM (1.1.4) ice sheet model and the MOM5 (5.1.0) ocean model via the PICO ice shelf cavity model in an Antarctic domain

Moritz Kreuzer<sup>1,2</sup>, Ronja Reese<sup>1</sup>, Willem Nicholas Huiskamp<sup>1</sup>, Stefan Petri<sup>1</sup>, Torsten Albrecht<sup>1</sup>, Georg Feulner<sup>1</sup>, and Ricarda Winkelmann<sup>1,2</sup>

<sup>1</sup>Earth System Analysis, Potsdam Institute for Climate Impact Research (PIK), Member of the Leibniz Association, 14412 Potsdam, Germany

<sup>2</sup>Institute of Physics and Astronomy, University of Potsdam, 14476 Potsdam, Germany

**Correspondence:** Moritz Kreuzer (kreuzer@pik-potsdam.de) and Ricarda Winkelmann (ricarda.winkelmann@pik-potsdam.de)

Received: 9 July 2020 – Discussion started: 14 September 2020

Revised: 16 April 2021 – Accepted: 19 May 2021 – Published: 22 June 2021

**Abstract.** The past and future evolution of the Antarctic Ice Sheet is largely controlled by interactions between the ocean and floating ice shelves. To investigate these interactions, coupled ocean and ice sheet model configurations are required. Previous modelling studies have mostly relied on high-resolution configurations, limiting these studies to individual glaciers or regions over short timescales of decades to a few centuries. We present a framework to couple the dynamic ice sheet model PISM (Parallel Ice Sheet Model) with the global ocean general circulation model MOM5 (Modular Ocean Model) via the ice shelf cavity model PICO (Potsdam Ice-shelf Cavity mOdel). As ice shelf cavities are not resolved by MOM5 but are parameterized with the PICO box model, the framework allows the ice sheet and ocean components to be run at resolutions of 16 km and 3° respectively. This approach makes the coupled configuration a useful tool for the analysis of interactions between the Antarctic Ice Sheet and the global ocean over time spans of the order of centuries to millennia. In this study, we describe the technical implementation of this coupling framework: sub-shelf melting in the ice sheet component is calculated by PICO from modelled ocean temperatures and salinities at the depth of the continental shelf, and, vice versa, the resulting mass and energy fluxes from melting at the ice–ocean interface are transferred to the ocean component. Mass and energy fluxes are shown to be conserved to machine precision across the considered component domains. The implementation is com-

putationally efficient as it introduces only minimal overhead. Furthermore, the coupled model is evaluated in a 4000 year simulation under constant present-day climate forcing and is found to be stable with respect to the ocean and ice sheet spin-up states. The framework deals with heterogeneous spatial grid geometries, varying grid resolutions, and timescales between the ice and ocean component in a generic way; thus, it can be adopted to a wide range of model set-ups.

## 1 Introduction

Most of Antarctica's coastline is comprised of floating ice shelves where glaciers of the Antarctic Ice Sheet drain into the surrounding Southern Ocean. Mass loss of these ice shelves occurs through ocean-induced melting at their base and calving of icebergs which both contribute about the same amount (Depoorter et al., 2013). Observations show that ice shelf–ocean interaction has been the main driver for mass loss of the West Antarctic Ice Sheet for the past 25 years (Jenkins et al., 2018; Shepherd et al., 2018; Holland et al., 2019). Ocean forcing has also been identified as playing a major role in past changes of the Antarctic Ice Sheet. Evidence that the Holocene retreat of the West Antarctic Ice Sheet was driven by warm water intrusions onto the continental shelf was provided by the palaeo-proxy data analysis of Hillenbrand et al. (2017) and supported by ensemble

modelling for the Ross Embayment (Lowry et al., 2019). Ice sheets respond to changing oceanic and atmospheric conditions, but they also feed back to the Earth's climate in various ways, including through meltwater input into the oceans, sea level change, or change in atmospheric circulation and precipitation patterns resulting from changes in orography and albedo (Nowicki et al., 2020; Vizcaíno et al., 2014). To study interactions and feedbacks between the Antarctic Ice Sheet and the ocean, such as through melt-induced freshwater input into the ocean, numerical models are an important tool. As the large ice sheets have long response timescales, coupled simulations over millennia are necessary to capture long-term effects. Such coupled simulations are also useful to study the long-term past or future evolution of ice sheets and oceans. This, together with the advantage of using ensemble simulations to constrain uncertainty in parameterized processes, makes computational efficiency a key requirement for such coupled models.

Existing land ice–ocean modelling approaches can be classified in five major categories which will be briefly introduced below:

1. global ocean and/or atmosphere models with fixed ice sheets;
2. stand-alone ice sheet models with simplified ocean forcing;
3. high-resolution ocean models resolving ice shelf cavity geometries;
4. high-resolution, regional coupled ice–ocean models;
5. global, coarse-grid ice–ocean coupled models with simplified ice–ocean interactions.

The standard set of experiments for the Coupled Model Intercomparison Projects (CMIPs) are performed by atmosphere–ocean general circulation models which use fixed, non-dynamic ice sheet configurations and, therefore, only have a limited representation of the aforementioned interactions and feedbacks (category 1; e.g. Eyring et al., 2016). CMIP-style models are computationally demanding which usually limits their application to centennial timescales (Balaji et al., 2017). For transient runs beyond the 21st century, however, fixed ice sheets would be an unrealistic assumption.

Ice dynamics missing in stand-alone climate models are traditionally computed by stand-alone ice sheet models (category 2), as ice dynamics typically respond on centennial to millennial timescales. These simulations rely on external forcing, most notably for atmospheric and oceanic boundary conditions. Ocean forcing is applied either through prescribed melt rates or through parameterizations of various complexity based on temperature, salinity, or pressure (see e.g. Asay-Davis et al., 2017, for a more in-depth discussion). The latter approach is used, for instance, in the Ice

Sheet Model Intercomparison Project for CMIP6 (ISMIP6; Nowicki et al., 2020; Seroussi et al., 2020; Jourdain et al., 2020), where stand-alone ice sheet models are forced by atmospheric and oceanic boundary conditions from CMIP5 (Taylor et al., 2012) to constrain Antarctic mass loss and sea level rise until the end of the century.

The low computational cost of melt parameterizations for stand-alone ice sheet models allows experiments to be integrated on multi-millennial timescales. However, this comes with uncertainties in oceanic boundary conditions not only due to the absence of a dynamic ocean but also due to missing feedbacks between ice and ocean.

A much more detailed representation of the ice–ocean boundary layer processes is achieved with high-resolution, cavity-resolving ocean models (category 3). Usually, this model type simulates the ice shelf geometry as static but thermodynamically active (e.g. Donat-Magnin et al., 2017). Their application ranges from idealized-geometry set-ups to specific regions like the Weddell or Amundsen seas and even circum-Antarctic set-ups. High-resolution ocean modelling (horizontal resolution of the order of 1–10 km) is needed to capture the complex processes determining the water masses that access the ice shelf cavities and the amount of heat that is available for melting the ice. A detailed discussion of these processes including a list of available models is given in Diniman et al. (2016).

Closely related to ice shelf cavity-resolving ocean models are coupled ice–ocean high-resolution models (category 4), which include an additional representation of grounded and floating ice dynamics. These models have been applied to idealized geometries (e.g. De Rydt and Gudmundsson, 2016) or regional set-ups (e.g. Naughten et al., 2021; Seroussi et al., 2017; Timmermann and Goeller, 2017). They can also be used to assess simple melt parameterizations from category 2 (e.g. Favier et al., 2019).

While the detailed representation of sub-shelf processes is important for realistic estimates of melt rates, these highly resolved configurations are, because of their computational demand, not practical to examine long-term and global effects of ice–ocean interaction.

This is, however, crucial because including freshwater fluxes from the Antarctic Ice Sheet in simulations of global circulation models has been shown to influence global ocean temperatures and their variability, to impact precipitation patterns, and to increase Antarctic ice loss through trapping warm water below the sea surface (Bronselaeer et al., 2018; Golleger et al., 2019). To study these effects on long timescales, a relatively new type of model is useful: large-scale ice–ocean models coupled via simplified melt parameterizations (category 5). Examples of global ocean-ice sheet coupling approaches are given in Goelzer et al. (2016) and Ziemen et al. (2019). Both of the above-mentioned studies use melt parameterizations that describe the melt process directly at the ice–ocean interface (Beckmann and Goosse, 2003; Holland and Jenkins, 1999). In addition to the melt-

ing at the ice–ocean interface, the Potsdam Ice-shelf Cavity mOdel (PICO; Reese et al., 2018) mimics the large-scale overturning circulation in ice shelf cavities. PICO can model melt rates in accordance with observations (Rignot et al., 2013): while average melt rates in cold cavities, such as underneath Filchner–Ronne Ice Shelf, are of the order of  $1 \text{ m a}^{-1}$ , melt rates in warm cavities, such as those found in the Amundsen Sea, are of the order of  $10 \text{ m a}^{-1}$ . At the same time PICO is computationally efficient compared with high-resolution, cavity-resolving ocean models. So far PICO has been used for stand-alone ice sheet modelling (category 2 from above e.g. in Reese et al., 2020, and Albrecht et al., 2020); however, as PICO is driven by far-field ocean temperature and salinity in front of the ice shelf cavities, it can also act as a coupler between non-cavity-resolving ocean models and ice sheet models.

To study the ice sheet and ocean system on a global and multi-millennial scale, we present a category 5 framework for the dynamical coupling of the Parallel Ice Sheet Model (PISM; Bueller and Brown, 2009; Winkelmann et al., 2011) and a coarse-resolution configuration of the Modular Ocean Model (MOM5; Griffies, 2012) using PICO. The design of the presented framework follows three criteria: (1) mass and energy conservation needs to be ensured over both ocean and ice sheet component domains, (2) the coupling framework should not introduce a performance bottleneck to the existing stand-alone models, and (3) the framework should follow a generic and flexible design independent of specific grid resolutions or number of deployed CPUs.

In the following, we introduce the ice sheet and ocean components in use, including their grid definitions (Sect. 2). The framework design including the variables that are exchanged between the components is discussed in Sect. 3, followed by a detailed description of inter-component data processing in Sect. 4. The framework's computational performance, conservation of mass and energy, and results of coupled simulations for present-day conditions are evaluated in Section 5, followed by a discussion (Sect. 6) and conclusions (Sect. 7).

## 2 Models

The following paragraphs introduce the PISM ice sheet model including its sub-shelf cavity model PICO and the MOM5 ocean model, which are coupled as components into the framework.

### 2.1 The PISM ice sheet model and the PICO ice shelf cavity model

The Parallel Ice Sheet Model<sup>1</sup> (PISM) is an open-source model that simulates ice sheets and ice shelves using a finite-difference discretization (Bueller and Brown, 2009; Winkel-

mann et al., 2011). PISM is defined on a regular Cartesian grid as shown in Fig. 1a, which is projected on a WGS84 ellipsoid (Slater and Malys, 1998) or related geometries like a perfect sphere. In this work PISM is used with a horizontal resolution of  $16 \text{ km} \times 16 \text{ km}$  with 80 vertical levels (Albrecht et al., 2020). The vertical resolution increases from 130 m at the top of the domain to 20 m at the (ice) base, with a domain height of 6000 m. PISM uses a hybrid of the shallow-ice approximation (SIA) and the two-dimensional shelfy-stream approximation of the stress balance (SSA, MacAyeal, 1989; Bueller and Brown, 2009) over the entire Antarctic Ice Sheet. The grounding line position is determined using hydrostatic equilibrium, with sub-grid interpolation of the friction at the grounding line (Feldmann et al., 2014).

PISM is a thermomechanically coupled (polythermal) model based on the Glen–Paterson–Budd–Lliboutry–Duval flow law (Aschwanden et al., 2012). The three-dimensional enthalpy field can evolve freely for given boundary conditions. We apply a power law for sliding with a Mohr–Coulomb criterion relating the yield stress to parameterized till material properties and the effective pressure of the overlying ice on the saturated till (Bueller and van Pelt, 2015). Basal friction and sub-shelf melting are linearly interpolated on a sub-grid scale around the grounding line (Feldmann et al., 2014). The calving front position can evolve freely using the eigen-calving parameterization (Levermann et al., 2012) which is combined with the removal of ice that is thinner than 50 m.

The numerical time-stepping scheme is adaptive and based on the Courant–Friedrichs–Lewy (CFL) condition among others (Bueller et al., 2007), which results in a range of time steps from minutes to years depending on the physical state of the model. The PISM source code is written in C++.

The Potsdam Ice-shelf Cavity mOdel (PICO) calculates sub-shelf melt rates and is implemented as a sub-module of PISM (Reese et al., 2018). It parameterizes the vertical overturning circulation in ice shelf cavities driven by the ice pump mechanism, as described by Lewis and Perkin (1986). This circulation induces melting and freezing below the ice shelves, as sketched in Fig. 3. PICO uses a box representation below the ice shelves developed by Olbers and Hellmer (2010) and extends their approach to two horizontal dimensions. Input for PICO are ocean temperature and salinity at the depth of the continental shelf. The strength of the overturning circulation is calculated in PICO from the density difference between the inflowing water masses and the water masses in the first box close to the grounding line and scaled with a continent-wide overturning coefficient, which is an internal PICO parameter. Thus, velocities of water masses flowing into the ice shelf cavities are not required.

<sup>1</sup>see <https://pism-docs.org/> (last access: 16 April 2021)

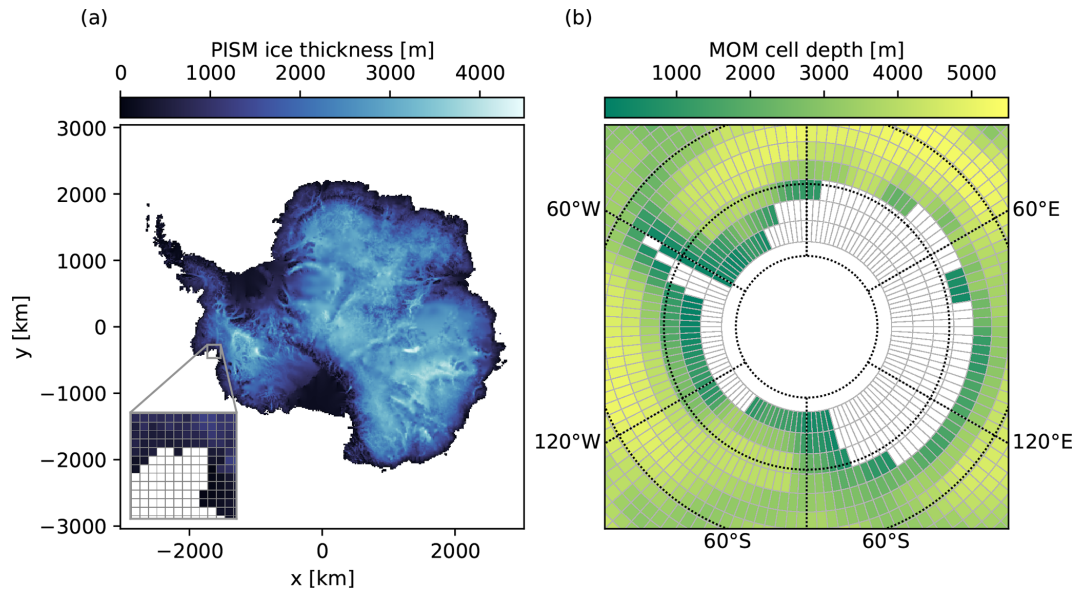


**Figure 1.** Ice sheet and ocean component grids. **(a)** Ice thickness in Antarctica on the Cartesian PISM grid. The inset shows the grid structure in a coastal area for a resolution of 16 km. **(b)** Depth of MOM5 cells displayed in a stereographic projection centred at the South Pole. Resolution at 70° S is  $\sim 3^\circ$  lat  $\times 3^\circ$  long ( $\sim 330$  km  $\times 115$  km). White cells are considered land by MOM5. The ocean grid extends to 78° S. Interlocking of PISM and MOM5 domains is shown in Figs. 3 and 6a.

## 2.2 The MOM5 ocean model

The ocean component in use for this coupling set-up is the Modular Ocean Model v5<sup>2</sup> (MOM5; Griffies, 2012) which is an open-source, three-dimensional ocean general circulation model. It is coupled via the Flexible Modelling System (FMS) coupler to the Sea Ice Simulator (SIS; Winton, 2000). In this work, we also include SIS and FMS when referring to MOM5.

For this study, MOM5 is used with a global coarse grid set-up from Galbraith et al. (2011, see Fig. 1b): the lateral model grid is 3° resolution in longitude (120 cells), and it varies in latitude from 3° at the poles to 0.6° at the Equator (80 cells). It makes use of a tripolar structure to avoid the grid singularity at the North Pole (Murray, 1996). The vertical grid is defined using the rescaled pressure coordinate ( $p^*$ ) with a maximum of 28 vertical layers. The uppermost eight layers are approximately 10 m thick, gradually increasing for deeper cells to a maximum of ca. 511 m. The vertical resolution at depths relevant for ice shelf cavities is between 50 and 180 m. The lowermost cells can have a reduced thickness to account for ocean bathymetry with partial cells. The ocean grid is not defined in the centre of the Antarctic continent (south of  $\approx 78^\circ$  S; see Fig. 1b). The ocean–sea ice system time steps are set to 8. MOM5, SIS, and FMS are written in Fortran.

## 3 Coupling approach

The design of the coupling between the PISM ice sheet component and the MOM5 ocean component is shown in Fig. 2, including the exchanged variables. PICO uses two-dimensional (horizontal) input fields, namely temperature and salinity of water masses that access the ice shelf cavities, to calculate melting and refreezing at the ice–ocean interface, as illustrated in Fig. 3. Fluxes describing basal melt, surface runoff, and calving in the ice component are used to determine the mass as well as energy fluxes received by the ocean component.

The timescales of physical processes as well as the numerical time steps in MOM5 (hours) and PISM (years) differ by several orders of magnitude. This is one motivation among others to use an *offline sequential coupling* approach to exchange the fields between the two components. In this case, both components are run in alternating order for the same model time, which will be referred to as the *coupling time step*. This technical procedure is illustrated in Fig. 4. An alternative *online coupling* approach is discussed in Sect. 6. In the offline coupling procedure, one component is first run for the period of a coupling time step. The output is then processed and provided as input or a boundary condition to the other component. Using the modified input, the components are restarted from their previous computed state. For example, MOM5 runs for 10 years and writes annual mean diagnostics fields of temperature and salinity. PISM receives the temporal average of these fields over the coupling time step as boundary conditions for PICO and is then integrated

<sup>2</sup>see <https://mom-ocean.github.io/> (last access: 16 April 2021)

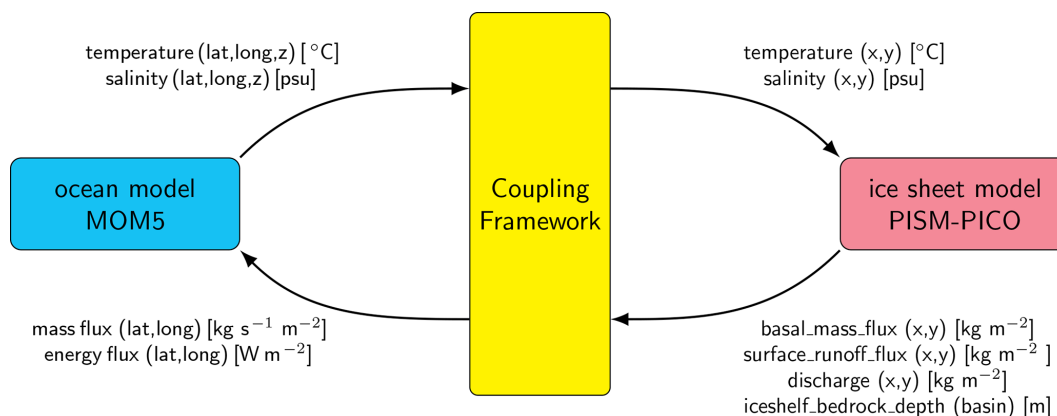


**Figure 2.** Overview of the coupling framework showing the input and output variables for the MOM5 ocean component and the PISM ice sheet component. Dimensions of variables are given in parentheses, and units are given in square brackets. The (lat, long) coordinates refer to the spherical ocean component grid, and the (x, y) coordinates refer to the Cartesian ice sheet component grid.

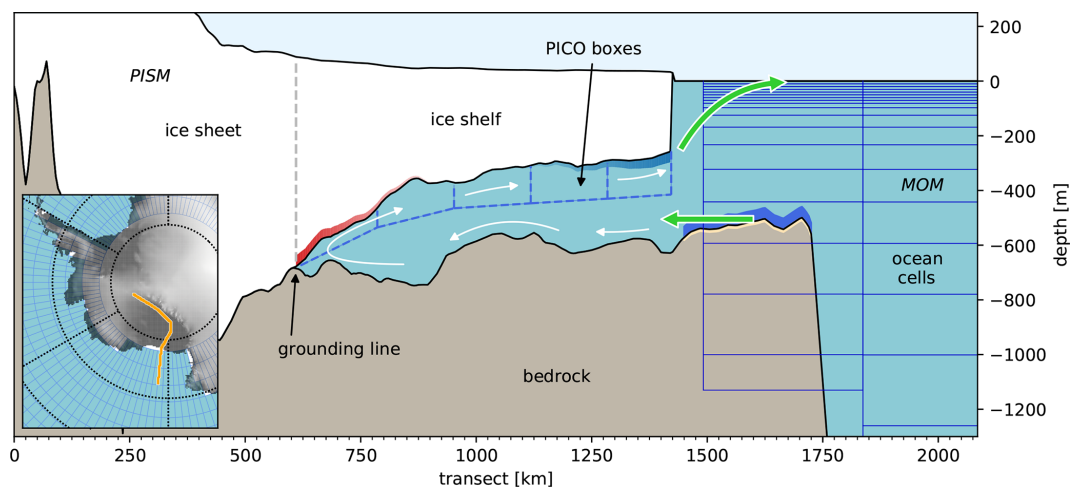


**Figure 3.** Coupling framework for the PISM ice sheet component and the MOM5 ocean component via the PICO ice shelf cavity model. A cross section of PISM bedrock (brown) and ice thickness (white) is compared to the MOM5 ocean cells (blue continuous lines). The inset shows the transect line (in orange) in the Antarctic region. PICO boxes (blue dashed lines) follow the overturning circulation in the ice shelf cavity. The circulation is indicated by white arrows with the highest melting in the deepest regions close to the grounding line (red shading) and lower melting or refreezing in the shallower areas towards the ice shelf front (blue shading). The exchange of variables and fluxes between the two components is indicated by green arrows: PICO input from MOM5 is taken at the depth of the continental shelf (dark blue regions). Mass and energy fluxes from PICO are transferred to MOM5 through the surface runoff interface.

for the same 10-year period. Melt water and energy fluxes derived from PISM output are aggregated over the coupling time step. The resulting fluxes are then added as external fluxes to the ocean over the course of the next integration period. To avoid shocks in the forcing, they are distributed uniformly over the entire coupling time step.

The coupling framework consists of a Bash script that implements the coupling procedure indicated in Fig. 4, making use of the Climate Data Operator (CDO; Schulzweida, 2019) and netCDF Operator (NCO; Zender, 2018) software tools. The output processing between the different component executions is implemented in Python scripts. Their functionality will be explained in the next sec-

tion. The code is made available in a public archive (<https://doi.org/10.5281/zenodo.4692679>, Kreuzer, 2021a), and the reader is referred to the “Code and data availability” section for further information.

#### 4 Inter-component data processing

To make the output of the ocean component compatible with the input requirements of the ice component and vice versa, processing of data output fields, like regridding, adjustment of dimensions, unit conversion, or filling of missing values, is required, which is described in this section.



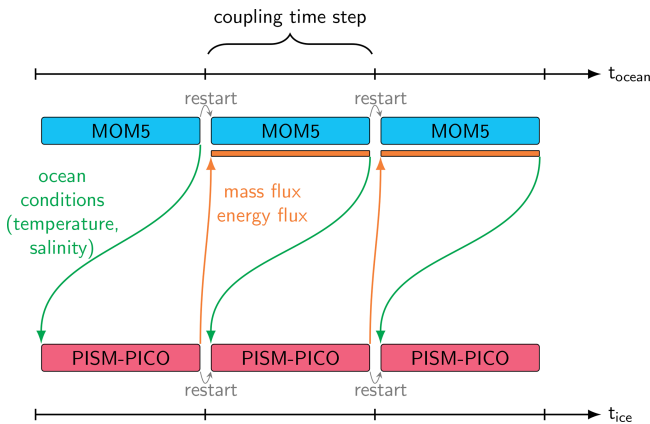


**Figure 4.** Offline coupling procedure for the PISM–MOM5 set-up: the components are run sequentially for the same coupling time step, and variables are exchanged after each run. Temperature and salinity variables from the MOM5 ocean component are used as input fields for the PISM–PICO ice component. Mass and energy fluxes from PISM–PICO output are uniformly applied over the next coupling time step as input to MOM5.

The ice and ocean components operate on independent, non-complementary computational grids. The inset of Fig. 3 shows that there are both spatial gaps and overlaps between the ocean grid cells and the ice extent represented by PISM. As the ocean grid is much coarser than the ice grid and MOM5 cells are either defined entirely as land or ocean (no mixed cells allowed), inconsistencies in the exchange of quantities between the two grids are unavoidable, requiring careful consideration of data regridding.

The grid remapping mechanisms presented in the following sections are independent of the used grid resolutions.

#### 4.1 Ocean to ice

PICO uses a definition of ocean basins around the Antarctic Ice Sheet which encompass areas of similar ocean conditions at the depth of the continental shelf (Reese et al., 2018). They are based on Antarctic drainage basins defined in Zwally et al. (2012) and extended to surrounding ice shelves and the Southern Ocean (see Fig. 5b). Oceanic fields of temperature and salinity are averaged over the continental shelf for each basin and provided as input to PICO. Note that PICO uses one value of temperature and salinity per basin.

Three steps are needed to process the oceanic output fields to make them usable as input to PISM:

- First, the three-dimensional output fields (temperature and salinity) are remapped bilinearly from the spherical ocean grid to the Cartesian ice grid. Bilinear regridding is chosen to allow for a smooth distribution of the coarse ocean cell quantities on the finer ice grid. Only regions with valid ocean data are filled on the ice grid, which is up to the cell centre of the southernmost ocean cell.

Areas with missing data need to be filled accordingly (compare grey areas in Fig. 5a, for example), which is done in the next step. Another option – linear extrapolation into areas with no ocean data coverage by the bilinear regridding scheme – is not applied here as it can lead to unrealistic results.

- Secondly, missing values are filled with appropriate data, namely the average over all existing values that are adjacent to grid cells with missing values. This procedure is conducted for each basin and vertical layer, using the same mean value of adjoining valid cells for all missing grid cells in that basin. Now, the continental shelf area between the ice shelf front and the continental shelf break (see Fig. 5a), which is used by PICO to calculate the basin mean values of oceanic boundary conditions, is entirely filled with appropriate values.
- Lastly, the three-dimensional variables are reduced to two-dimensional PICO input fields which represent the ocean conditions at the depth of the continental shelf. This is done by vertical linear interpolation: for every horizontal grid point, the data are interpolated to PISM’s mean continental shelf depth of the corresponding basin. If the ocean bathymetry is shallower than the continental shelf depth as seen by PISM, the lowermost ocean layer is chosen. An example of the processed input data for PICO is shown in Fig. 5b.

#### 4.2 Ice to ocean

To transfer the mass and energy fluxes from the ice component to the ocean component, a mapping from the PISM to the MOM5 grid is required. There are large areas of the PISM domain that are not overlapping with valid MOM5 ocean cells (see white areas in Fig. 1b and the inset in Fig. 3). To ensure mass and energy conservation, we introduce a new mechanism for the coupled system which maps every southernmost ocean cell of the MOM5 grid to exactly one PICO basin (see Fig. 6). The mechanism selects the basin that the centre of the MOM5 cell lies in. As one basin is usually linked to multiple ocean cells, the link proportion between each basin and their corresponding ocean cells is scaled by the ocean cell areas. An example for PISM mass fluxes and their distribution onto the MOM5 grid is shown in Fig. 7.

The mass and energy fluxes from PISM output are calculated and distributed in the following manner:

- The PISM output variables describing the surface runoff, basal mass fluxes, and discharge through calving are added up. As they are given in units of kilograms per square metre per year ( $\text{kg m}^{-2} \text{yr}^{-1}$ ), multiplication by the PISM grid cell areas and division by number of seconds per year transforms the consolidated mass flux into units of kilograms per second ( $\text{kg s}^{-1}$ ).

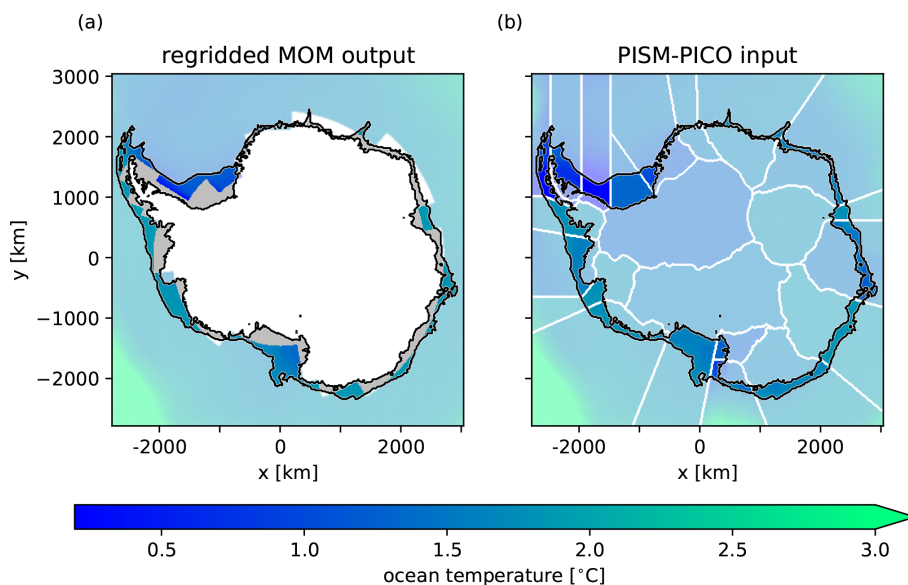


**Figure 5.** Visualization of inter-component data processing from (a) regrided ocean component output to (b) ice component input. In panel (a), an example is shown for the ocean temperature field at a depth of approximately 500 m, with black contour lines indicating the continental shelf between the ice shelf front and the continental shelf break ( $-2000$  m) as used in PICO. Missing values within that area are coloured in grey. Ocean values outside the continental shelf are not used for averaging basin mean values in PICO and are therefore shown using lighter colours. The result of the processing procedure is the two-dimensional ocean temperature field shown in panel (b), which is obtained through vertical interpolation of the filled fields applied to appropriate basin depths. PICO basins are indicated by white contour lines.

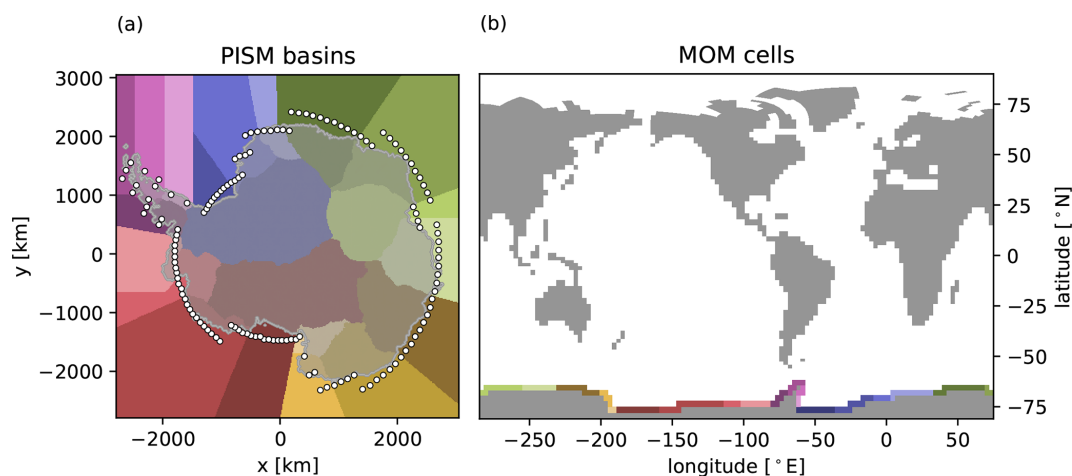


**Figure 6.** Visualization of the mapping mechanism between (a) PICO basins and (b) MOM5 ocean cells. PICO basins on the ice sheet grid are shown in panel (a), with each basin assigned a different colour. The location of the centre of southernmost ocean cells is denoted by white circles. As a spatial reference, the ice cover modelled by PISM is shown in grey. Panel (b) shows the MOM5 land–ocean mask with corresponding PICO basin colours for the southernmost ocean cells surrounding the Antarctic Ice Sheet. Grey cells are considered as land in MOM5.

- The energy flux from ice to ocean is obtained by multiplying the mass flux resulting from basal melt and discharge by the enthalpy of fusion ( $L = 3.34 \times 10^5 \text{ J kg}^{-1}$ ) to account for the energy required during the phase change from frozen to liquid state or vice versa. At this point, the energy flux is in watts (W). Potential diffu-

sive heat fluxes from the ocean into the ice as well as the energy required to warm the melt water to ambient temperatures are comparatively small (Holland and Jenkins, 1999) and, thus, neglected here.

- Having calculated bulk mass and energy fluxes, they can be aggregated for each PICO basin and distributed to

the corresponding ocean cells with the mapping mechanism described above. On the ocean grid, the fluxes are divided by the given grid cell area resulting in units of kilograms per second per square metre ( $\text{kg s}^{-1} \text{m}^{-2}$ ) for mass and watts per square metre ( $\text{W m}^{-2}$ ) for energy fluxes. These fluxes are input into the ocean surface through MOM5's internal FMS coupler.

## 5 Evaluation

In this section, the coupling set-up will be evaluated on the basis of runtime performance and numerical accuracy. Physical evaluation of the coupled set-up is provided for present-day conditions. Further validation and implications in terms of possible feedback mechanisms will be studied in detail in a separate article.

### 5.1 Coupled benchmarks

The coupling framework presented here provides the tools for coupled ice sheet–ocean simulations on centennial to millennial timescales, which requires reasonably fast execution times. In the following, we analyse the coupled execution time and evaluate the efficiency of the coupling framework, using a total model runtime of 200 years on 32 cores (two CPU nodes, each equipped with two eight-core Intel E5-2667 v3). For the modelling of ice–ocean interactions, the coupling time step is an important parameter that requires careful adjustment, while keeping the different timescales of ice and ocean processes in mind. Overly short time steps certainly yield a waste of computation time and disc space for restart and coupling overhead, whereas overly long time steps could possibly yield instabilities and lead to a less accurate representation of ice–ocean interaction processes. Here, only the influence of the coupling frequency on the overall runtime performance is assessed, leaving the examination of physical implications to Sect. 5.3. Two experiments with time steps of 1 and 10 years are compared, with a total number of 200 and 20 coupling iterations respectively. The individual coupled component simulations start from quasi-equilibrium conditions.

The elapsed total runtime (wall-clock time) required for 200 years of model time is 21 976 and 13 245 s with a coupling time step of 1 and 10 years respectively. Figure 8 shows the runtime required for each of the individual components within the coupling framework, and the corresponding numbers are listed in Table A1. With a 10-year coupling time step, the core runtime of MOM5 (93 %) including necessary post-processing (2 %) requires the biggest share of total runtime in the coupled set-up. The PISM runtime (4 %) as well as the time needed for the coupling preprocessing (< 1 %) and inter-component processing (< 2 %) routines are almost negligible. This means that, in the given set-up, coupling the PISM ice sheet component to the MOM5 ocean com-

ponent comes with minimal overhead compared with stand-alone ocean simulations, when using a coupling time step of 10 years.

In the experiment using a yearly coupling time step, the elapsed time for all MOM5 executions increases slightly (15 446 s) compared with 10-yearly coupling (12 267 s). The increase is due to component initialization overhead which occurs 10 times as often as in the decennial coupling configuration. The ocean component post-processing (9 %) and inter-component processing routines (4 %) are taking a bigger share of the total runtime, as the number of executions has similarly increased by a factor of 10. PISM runtimes are about 6 times greater for yearly coupling (13 % of total runtime), although the total integration period in PISM is the same in both experiments. This is due to the component initialization as well as reading and writing of input and output and restart files dominating the PISM execution of 1 model year, which is reasonable as PISM is designed, and usually used, for much longer integration times. Overall, the total execution time increases by about 66 % in the yearly coupled set-up compared with the run with a coupling time step of 10 years.

### 5.2 Energy and mass conservation

In a coupled model, conservation of mass and energy is important to ensure that no artificial sources or sinks of these quantities are introduced through the coupling mechanism. This is especially important in the context of palaeo-modelling, where simulations can span tens of thousands of years. In the presented ice–ocean coupling framework, prescribed fluxes are applied at the open system boundaries (e.g. precipitation from the atmosphere to ice and ocean or river runoff from land to ocean). To check that the total amount of mass and energy stocks is constant in the coupled system over the model integration, we assess virtual quantities. Those are obtained by subtracting the masses applied through surface fluxes from the total mass and energy stocks calculated in the model (see Eq. 1 for mass). If the virtual model mass across the model components  $m_v$  is constant with fluctuations of the order of machine precision, as denoted in Eq. (2), conservation of mass is achieved.

$$m_v = (m_o + m_{si} - m_{osi}^s - m_{osi}^d) + (m_{li} - m_{li}^s) \quad (1)$$

$$\frac{d}{dt} m_v \sim 0 \text{ Gt a}^{-1} \quad (2)$$

The masses of the ocean, sea ice, and land ice components are represented by  $m_o$ ,  $m_{si}$ , and  $m_{li}$  respectively, whereas  $m_{osi}^s$  and  $m_{li}^s$  denote the cumulative, spatially integrated surface mass balance flux of the MOM5–SIS ocean–sea ice component and the PISM land ice component respectively. The internal model drift of mass in the coarse-grid MOM5–SIS set-up is described by  $m_{osi}^d$  ( $\approx 4 \times 10^{15}$  kg accumulated over 200 years) and needs to be considered in the computation of virtual model mass in Eq. (1). All terms in Eq. (1) are



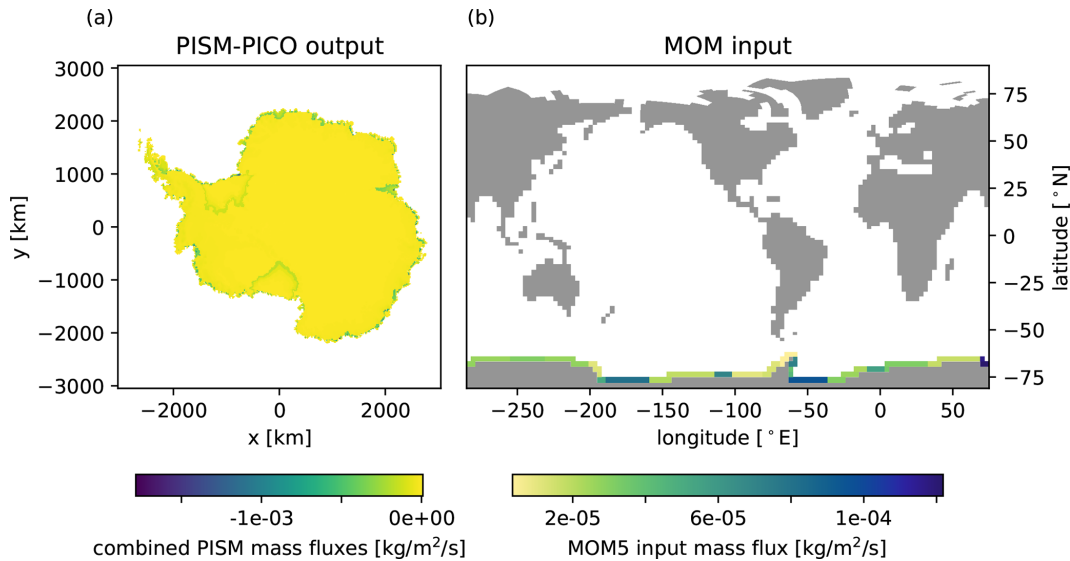


**Figure 7.** Visualization of (a) PISM mass flux distribution to (b) the MOM5 ocean grid. PISM output variables describing surface runoff, basal melting, and calving are aggregated over space and time (coupling time step) to calculate mass and energy fluxes which are processed as input to the MOM5 ocean component as described in Sect. 4.2. Panel (b) shows the corresponding mass flux distribution on the MOM5 grid.

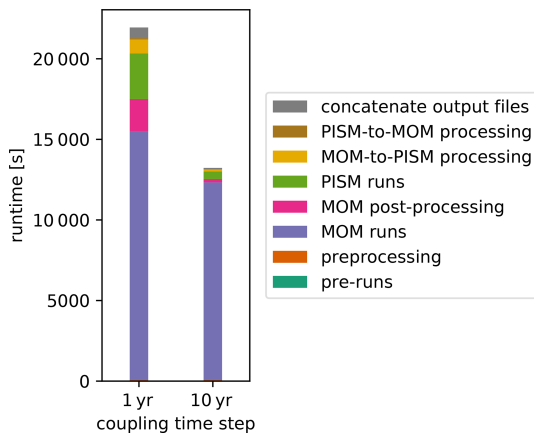


**Figure 8.** Runtimes of the coupled PISM–MOM5 set-up for 200 years of model time, using 32 cores and coupling time steps of 1 and 10 years. PISM runtimes include PICO, and MOM5 runtimes include SIS and FMS components. The elapsed time for individual components of the coupling framework is aggregated and stacked in the same order as in the legend. The runtimes are listed in Table A1.

quantities of mass with the temporal resolution of the coupling time step. The relative mass conservation error  $e_{rel}^m$  is calculated as fluctuations of the virtual model mass compared to its temporal mean  $\overline{m_v}$ , noted in Eq. (3).

$$e_{rel}^m = \frac{m_v - \overline{m_v}}{\overline{m_v}} \quad (3)$$

The relative mass conservation error  $e_{rel}^m$  is shown in Fig. 9a for 200 model years with a yearly coupling time

step. Regarding the order of magnitude of land ice mass  $\mathcal{O}(m_{li}) = 10^{19}$  kg, which is given in single precision ( $\approx 7$  decimal digits) output format, and the order of magnitude of ocean and sea ice mass  $\mathcal{O}(m_o + m_{si}) = 10^{21}$  kg, given in double precision ( $\approx 16$  decimal digits) format, the shown fluctuations of the order of  $10^{-9}$  are reasonable. As the relative mass error does not show a trend, no systematic error is introduced through the coupling procedure. In Fig. 9b, the fluctuations of virtual model mass is also compared to the mass flux between the land ice and ocean component ( $m_x$ ), which is of the order of  $\mathcal{O}(10^{-3})$ .

As PISM does not provide diagnostic variables to record incoming and outgoing energy fluxes across its modelled boundaries, an analysis of the total amount of enthalpy in the coupled ice–ocean system could not be easily derived. However, it is possible to show that no systematic error is induced during remapping the energy flux from the PISM to MOM5 grid. Figure 9c shows the relative energy flux remapping error of the test run undertaken in Sect. 5.1, which is of the order of double machine precision  $\mathcal{O}(1e^{-16})$ .

### 5.3 Coupled runs for present-day conditions

Here, we present a 4000 year (4 kyr) simulation of the coupled system under constant climate forcing for validation of the model. MOM5–SIS is forced by present-day monthly mean fields for radiation, precipitation, surface air temperature, pressure, humidity, and winds, as described in Griffies et al. (2009), with an internal coupling time step of 8 h between ocean and sea ice sub-components. River runoff from land in Antarctica is replaced by PISM fluxes. PISM is ini-

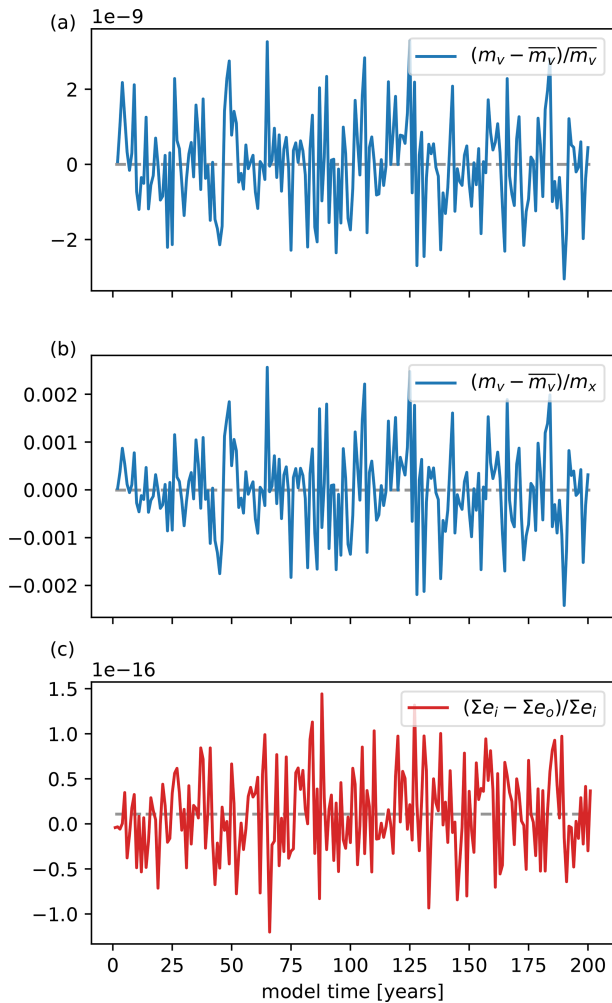


**Figure 9.** Mass and energy conservation. **(a)** Relative error of virtual mass progression in the coupled ice–ocean system which excludes mass changes applied through surface fluxes and the internal model drift of the coarse grid MOM5–SIS set-up. **(b)** A comparison of virtual mass fluctuations to the mass exchanged between ocean and land ice components ( $m_x$ ). **(c)** Relative error through remapping energy flux from the PISM to MOM5 grid, where  $e_i$  and  $e_o$  describe the transferred energy fields (unit W) on the land ice and ocean grid respectively.  $\Sigma e$  is the spatially aggregated energy over the whole grid domain.

tialized from Bedmap2 geometry (Fretwell et al., 2013), with surface mass balance and surface temperatures from RACMOv2.3p2 averaged between 1986 and 2005 (van Wessem et al., 2018). Geothermal heat flux is from Shapiro and Ritzwoller (2004). In the spin-up of PISM, PICO is used to calculate basal melt rate patterns underneath the ice shelves and driven by observed ocean temperature and salinity values on the continental shelves (1975–2012, Schmidtke et al., 2014).

Spin-up states for ocean and ice models are computed separately prior to coupling for 10 and 210 kyr respectively. To reduce a shock from changes in the river runoff boundary

conditions when starting the coupled simulation, mass and heat fluxes from the last 1 kyr of the ice sheet spin-up are included in the last 5 kyr of ocean spin-up. The initial ice spin-up was done for 200 kyr with PISM v1.0 (similar to Seroussi et al., 2017) and continued for another 10 kyr with the updated PISM v1.1.4. Ocean temperatures around Antarctica show a warm bias between 0.9 and 3.7 °C, which is too warm to maintain a stable ice sheet when coupled to PISM. Temperature and salinity fields are therefore modified by employing an anomaly method similar to Jourdain et al. (2020). From the ocean fields modelled by MOM5, anomalies relative to the last 100 years of the spin-up are calculated. These anomalies are then applied to the observational input used to drive PICO in the ice sheet spin-up. With this method, the ocean forcing for the ice sheet remains close to the stable forcing as long as the ocean state is not altered.

Starting from the spin-up ice and ocean states, two different coupled experiments are conducted for 4 kyr, both using a 10-year coupling time step. One set-up provides the mean ocean forcing over the coupling time step to the ice model, whereas the other uses a time series forcing of annual averaged ocean temperature and salinity and, thus, reflects the ocean forcing variability of a yearly coupling time step. Results of both experiments are shown in Fig. 10, including the last 5 kyr of stand-alone spin-ups for comparison. To analyse the ocean state, the following metrics are used: total ocean heat content (Fig. 10a); average of ocean model potential temperatures and salinities in southernmost cells at 400 m depth (Fig. 10b, e); Atlantic Meridional Overturning Circulation (AMOC; Fig. 10c), defined as the maximum annual mean of North Atlantic overturning between 20 and 90° N and below 500 m; Pacific deep temperature (Fig. 10d), which is the ocean potential temperature below 3000 m in the area from 110° E to 80° W and 10° S to 70° N; and Antarctic Bottom Water Formation (AABW; Fig. 10f), which is defined as the maximum annual mean of overturning between 90 and 0° S and below 2000 m. The state of the Antarctic Ice Sheet is analysed with the following metrics: ice volume above flotation (Fig. 10g); total area of grounded and floating ice (Fig. 10h, i); grounding line movement (Fig. 10j) as the mean of minimum distance between modelled grounding line and Bedmap2 data in every grounding line grid cell; ice thickness evolution (Fig. 10k) as root-mean-squared error (RMSE) of modelled grounded ice thickness compared with Bedmap2 data; and surface velocity deviation (Fig. 10l), defined as the RMSE of modelled surface velocities above 100 myr<sup>-1</sup> compared with Ice Velocity Map, v2 (Rignot et al., 2017, 2011; Mouginot et al., 2012).

The coupled system remains in equilibrium for both scenarios (orange and green lines for ocean; gold and dark grey lines for ice state in Fig. 10) as no major drift can be observed in any of the ocean or ice metrics. Variability in ice volume above flotation (Fig. 10g) is in the range of 0.15 m before and after coupling. The same pattern is observed in total ocean heat content (Fig. 10a) and Pacific deep tem-

perature (Fig. 10d), where the latter shows a variability of  $0.04^{\circ}\text{C}$ . Variations in Antarctic mean ocean temperatures are within  $0.1^{\circ}\text{C}$ . Changes in AMOC (Fig. 10c) and AABW (Fig. 10f) are in the range of 0.2 and  $0.6\text{ Sv}$  respectively, where  $1\text{ Sv} = 10^6\text{ m}^3\text{ s}^{-1}$ . Variability in the other ice metrics like grounded and floating area (Fig. 10h, i), grounding line deviation (Fig. 10j), ice thickness (Fig. 10k), and surface velocities (Fig. 10l) are comparable between coupled runs and the stand-alone spin-up. As no significant differences between the two scenarios can be observed, we are concluding that a coupling time step of 10 years is sufficient for coupled experiments that are in equilibrium. Whether this also holds for transient simulations is yet to be verified.

## 6 Discussion

The framework presented here to couple the PISM ice component to the MOM5 ocean component via PICO fulfils all three goals stated in Sect. 1: (1) mass and energy conservation across both component domains and (2) an efficient as well as (3) generic and flexible coupling framework design:

As described in Sect. 5.2, mass conservation across both component domains can be assured. Furthermore, the remapping scheme for energy fluxes is conservative as well. Compared with the required run time of MOM5, the framework routines are very efficient when choosing a coupling time step of 10 years. More frequent coupling causes a larger overhead, as reading and writing the complete model state of PISM to and from files is relatively expensive for very short simulation times. However, an increased ocean to ice forcing of 1 year does not affect the equilibrium state of the coupled system as shown in Sect. 5.3. The third criterion is fulfilled by the chosen offline coupling approach, which provides a generic and flexible design by making use of the component-related flexibility concerning grid resolution and degree of parallelization. This does not easily apply to the alternative approach of online coupling, which will be discussed below.

The chosen offline coupling framework executes the two different components alternately and independently, and manages the redistribution of the input and output files across the components as explained in Sect. 3. However, it is also conceivable to adopt an online coupling approach (also called synchronous coupling), where the ice and ocean component code are consolidated into one code structure. The exchange of variables between both components can subsequently take place through access to the same shared memory instead of writing the required variables to disc and reading from there again, as is done in offline coupling. This approach is used in studies such as Jordan et al. (2018). A comprehensive framework for online coupling of ocean and ice components is described in Gladstone et al. (2021). This coupling approach is especially powerful for high-resolution, cavity-resolving ice–ocean coupling, where frequent updates of the ice shelf cavity geometries and corresponding melt

rates are important. However, a prerequisite for online coupling is the adaptation of the stand-alone models for interactive execution of subroutines through a defined (external) interface. In the given case of coupling PISM and MOM5, this means that at least one of the two programs' code structure needs major modifications and modularization to equip the individual component parts, like initialization, time stepping routine, disc I/O (input and output), and stock checking, with suitable interfaces. This is independent of the chosen online coupling design (incorporating one code structure into the other or creating a new master program that governs both components). Synchronization of the PISM adaptive time step and the fixed ocean component time step would be a further issue, also keeping in mind that the comparably small ocean time step of a few hours is not applicable for the ice component: PISM can have a time step of around 0.5 years close to equilibrium with 16 km resolution due to the longer characteristic timescales of ice dynamics. The fact that both components are written in different programming languages (C++ and Fortran) imposes its own (although minor) barriers. A possible benefit of the described online coupling is less disc I/O overhead, which is especially relevant for small coupling time steps in the offline coupling approach (see Sect. 5.1); however, that does not outweigh the high initial and ongoing development effort which arises through writing and maintaining modified versions of the main component versions. Offline coupling comes with the advantage that only very minimal modifications of the existing components' source code are necessary. This makes it fairly easy to even replace the ice or ocean components in use with similar existing models, like using MOM5's successor MOM6. A further benefit of the offline coupling approach is that running several independent instances of PISM (e.g. for Antarctica and Greenland) at the same time can be easily implemented.

The coupling implementation exhibits certain simplifications that can be subject of future improvements. As described in Sect. 4.2, the mass and energy fluxes computed from PISM output are given as input to the ocean surface rather than being distributed throughout the water column – a limitation of MOM5's simplified treatment of all land-derived mass fluxes, including those from ice sheets. This simplification may affect vertical heat distribution and local sea ice formation (Bronse laer et al., 2018) as near-surface input generally makes the vertical column more stratified, whereas input below the mixed layer destabilizes the water column, thereby enhancing vertical mixing and extending the mixed layer depth (Pauling et al., 2016). A more realistic input depth into the ocean would be the lower edge of the ice shelf front (see start of upper green arrow in Fig. 3; Garabato et al., 2017) which could be determined as the average ice shelf depth of the last PICO box.

Mass and energy fluxes are composed of basal melting, surface runoff, and calving and are provided as input to the southernmost ocean cells (see Sect. 4.2). Icebergs can, how-

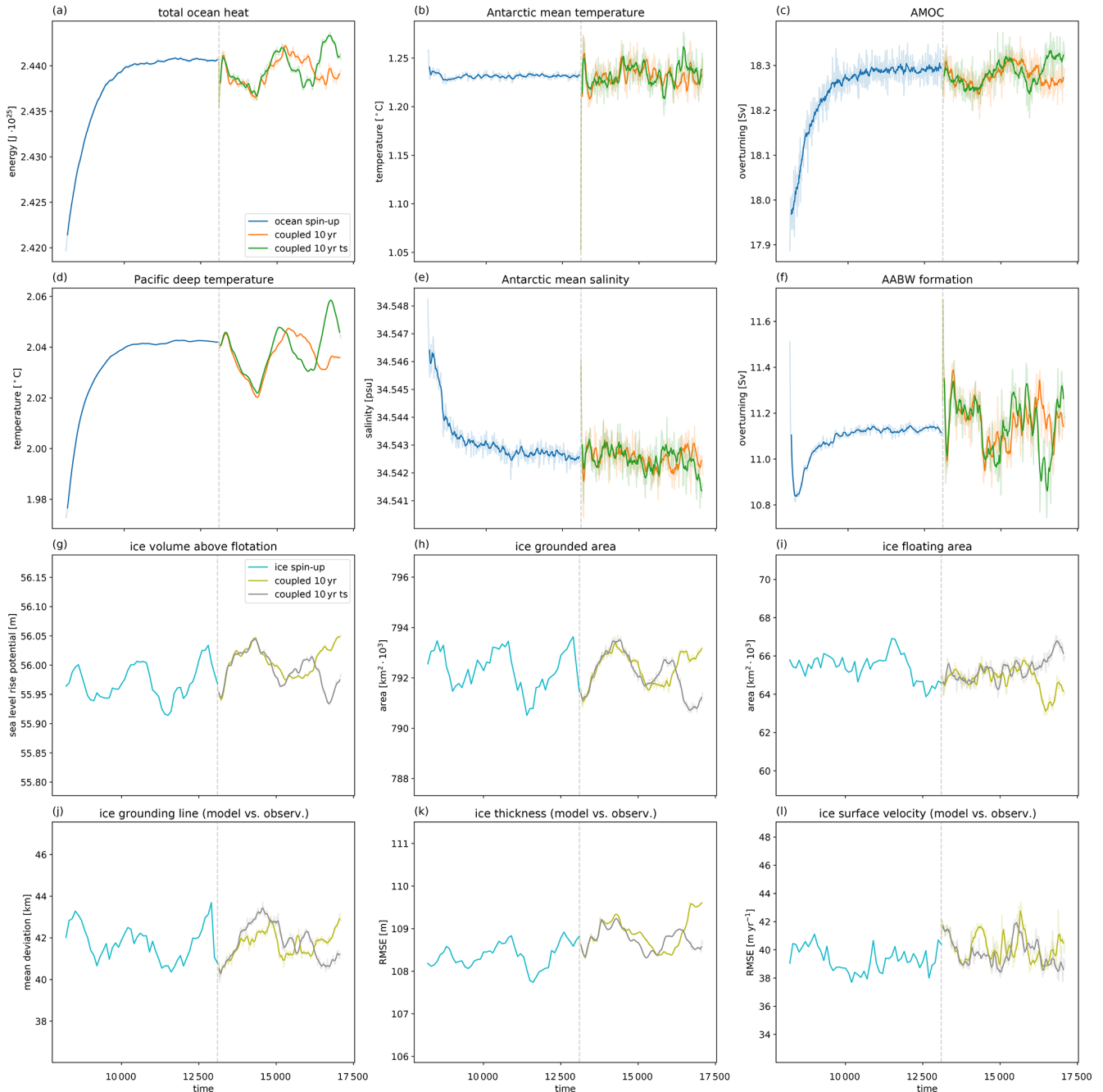


**Figure 10.** Evolution of the Antarctic Ice Sheet and the global ocean during spin-up and coupled simulations under constant climate forcing. Details about ocean (a–f) and ice metrics (g–l) are given in Section 5.3. Coupling starts at the vertical dashed line. Two coupling variants are presented, both using a coupling time step of 10 years, while one passes the time series of ocean forcing to the ice model (denoted as “ts”). Light and solid lines are 10- and 100-year running means respectively.

ever, travel substantial distances before they are completely melted and, thus, continuously distribute mass and energy fluxes into the ocean (Tournadre et al., 2016). The resulting spatial distribution of iceberg fluxes can introduce biases in sea ice formation, ocean temperatures, and salinities around Antarctica (Stern et al., 2016). Currently this is not consid-

ered in our framework and may be simulated by an additional iceberg component (as described in Martin and Adcroft, 2010) in the future.

Another simplification is contained in the energy flux description from ice to ocean. As explained in Sect. 4.2, the flux is calculated as the energy transferred through phase change

from frozen ice to liquid water. Diffusion of heat through the ice and energy required to warm up melt water to ambient ocean temperatures are currently not considered as they are estimated to be comparably small (Holland and Jenkins, 1999).

The waxing and waning of ice sheets on glacial–interglacial timescales causes the transfer of large amounts of water between the oceans and land ice sheets. Significant changes in sea level (120–135 m below present during the last glacial maximum; Clark and Mix, 2002) have large impacts on coastline positions. The response of the solid Earth component to changes in ice sheet mass has a similar effect. During long simulations the land–ocean mask needs to be adapted accordingly. As MOM5 cannot handle mixed ocean–land cells, which would allow for a smooth adaptation of a changing coastline, major changes in the land–ocean mask need to be performed during a transient simulation. This requires careful considerations like the initialization of newly flooded cells and implications concerning mass and energy conservation as well as model stability. The development of a sea-level-based dynamic ocean domain adaptation which applies the described changes to new ocean restart conditions is currently under way and will be incorporated in the described coupled set-up in the future.

In this study, we focus on the technical implementation of the coupling framework and evaluate it in a transient simulation under constant present-day climate forcing. As the ocean component has warm biases at intermediate depth around the Antarctic margin, we apply an anomaly approach to avoid unrealistic high melting and obtain physically meaningful simulations of the coupled system. We add anomalies from the ocean model component to observed temperatures, similar to the approach in ISMIP6 (Jourdain et al., 2020; Nowicki et al., 2020). The difficulties to accurately simulate Antarctic shelf dynamics and deep water formation in the Southern Ocean with ocean general circulation models is a long-standing issue for the ocean modelling community, with almost no models of the CMIP5 generation able to do this successfully (Heuzé et al., 2013). The improvement of these biases is the subject of ongoing work via the implementation and tuning of the new MOM6 ocean model. While the anomaly approach is appropriate for present-day simulations, for which we have observations, it is as yet unclear how these biases might be addressed for transient simulations on multi-millennial timescales. In the transient simulations, the effect of using a 10-yearly coupling time step was tested in a simulation with the variable 10-year ocean forcing being applied to the ice sheet instead of the 10-year average. We find that this variability has no effect in a steady-state simulation. These open issues, including the choice of the coupling time step under physical aspects, will be considered in a future study.

The presented coupling framework is characterized by a reduced-complexity approach. This is reflected, for instance, in the basin-wide averaging of PICO input which

does not account for horizontal differences such as cavity in- and outflow regions or modification of water masses on the continental shelf. Similarly, the complex processes determining whether upwelling Antarctic Circumpolar Deep Water reaches the continental shelf and the grounding lines (Nakayama et al., 2018) can only be partly represented due to the coarse bathymetric features of the MOM5 grid (see also Fig. 1b). However, the intermediate complexity of the coupled system enables ocean simulations on a global domain, opening possibilities to study interactions, feedbacks, and possible tipping behaviour on millennial timescales. Overall, despite the limitations discussed above, the coarse grid set-up of MOM5 in combination with the representation of the ice pump mechanism in PICO makes large-scale and long-term ice–ocean coupling possible at an intermediate level of complexity.

## 7 Conclusions

In this study, we focus on the technical approach and conservation aspects of coupling a large-scale configuration of the PISM ice sheet model and a coarse-grid-resolution set-up of the MOM5 ocean model via the PICO cavity model. This approach makes it possible to capture the typical overturning circulation in ice shelf cavities that cannot be modelled in global stand-alone ocean models. We can assure that conservation of mass and energy is obtained in the coupler between the ocean and land ice components while having a computationally efficient and flexible coupling set-up. Using this framework, which is openly available and can also be transferred to other ice sheet and ocean general circulation model components, feedbacks between the ice and ocean can be analysed in large-scale or long-term modelling studies. In future work, the physical processes and feedbacks between ice sheet, ice shelves, and ocean will be further analysed, and the interaction strengths can be evaluated on various timescales, from decades to multi-millennial simulations.

## Appendix A: Benchmark results

**Table A1.** Runtimes of the coupled PISM–MOM5 set-up for 200 years of model time using 32 cores. PISM runtimes include PICO, and MOM5 runtimes include SIS and FMS components.

Routine	One-year coupling		Ten-year coupling	
	Time (s)	Ratio (%)	Time (s)	Ratio (%)
Total	21 976.49	100.00	13 244.80	100.00
Pre-runs	24.17	0.11	24.41	0.18
Preprocessing	40.97	0.19	43.03	0.32
MOM runs	15 446.26	70.29	12 267.26	92.62
MOM post-processing	1993.09	9.07	205.98	1.56
PISM runs	2830.57	12.88	467.26	3.53
MOM-to-PISM processing	861.89	3.92	125.43	0.95
PISM-to-MOM processing	90.43	0.41	14.01	0.11
Concatenating output files	656.44	2.99	81.91	0.62



*Code and data availability.* The coupling framework code is hosted at [https://github.com/m-kreuzer/PISM-MOM\\_coupling](https://github.com/m-kreuzer/PISM-MOM_coupling) (last access: 16 April 2021). The exact version used in this paper has been tagged in the repository as v1.0.3 and is archived on Zenodo (<https://doi.org/10.5281/zenodo.4692679>, Kreuzer, 2021a).

The code makes use of the Climate Data Operator (CDO, version 1.9.6, Schulzweida, 2019; <https://doi.org/10.5281/zenodo.3991595>, Schulzweida et al., 2019) and the netCDF Operator (NCO, version 4.7.8, Zender, 2018; <https://doi.org/10.5281/zenodo.1490166>, Zender et al., 2018) software tools.

Version 1.1.4 of the Parallel Ice Sheet Model (PISM) was used (<https://doi.org/10.5281/zenodo.4686967>, Khrulev et al., 2021), and version 5.1.0 of the Modular Ocean Model (MOM) was used with slight modifications, as archived at <https://doi.org/10.5281/zenodo.3991665> (Leslie et al., 2020).

All data used in the tests detailed in this paper are archived at <https://doi.org/10.5281/zenodo.4692940> (Kreuzer, 2021b).

*Author contributions.* MK wrote and implemented the coupling framework and performed the analysis. RW, GF, and SP conceived the study. MK and RR designed the coupling strategy via PICO. SP and WH provided support with the set-up and use of MOM5. RR and TA provided support with the use of PISM. RR contributed to shaping the paper. MK prepared the paper with input and feedback from all co-authors.

*Competing interests.* The authors declare that they have no conflict of interest.

*Disclaimer.* Publisher's note: Copernicus Publications remains neutral with regard to jurisdictional claims in published maps and institutional affiliations.

*Acknowledgements.* Development of PISM is supported by NASA (grant no. NNX17AG65G) and NSF (grant nos. PLR-1603799 and PLR-1644277). The authors gratefully acknowledge the European Regional Development Fund (ERDF), the German Federal Ministry of Education and Research, and the Land Brandenburg for supporting this project by providing resources on the high-performance computer system at the Potsdam Institute for Climate Impact Research.

This work was supported by the Deutsche Forschungsgemeinschaft (DFG) in the framework of the priority programme “Antarctic Research with comparative investigations in Arctic ice areas” SPP 1158 by the following grants: grant no. WI 4556/4-1 (Moritz Kreuzer) and grant no. WI4556/2-1 (Torsten Albrecht). Ronja Reese was supported by the Deutsche Forschungsgemeinschaft (DFG; grant no. WI 4556/3-1) and through TiPACCs. The TiPACCs project has received funding from the European Union's Horizon 2020 Research and Innovation programme under grant agreement no. 820575. The work of Torsten Albrecht, Ricarda Winkelmann (grant no. FKZ: 01LP1925D), and Willem Nicholas Huiskamp (grant nos. FKZ: 01LP1504D and FKZ: 01LP1502C) has been conducted within the framework of the PalMod project, supported by the German Federal Ministry of Edu-

cation and Research (BMBF) as Research for Sustainability initiative (FONA).

We thank Paul Gierz from the Alfred-Wegener-Institut for in-depth discussions in the initial phase of this project. Significant parts of the work were done while Moritz Kreuzer was affiliated with the University of Potsdam (Department of Computer Science, August-Bebel-Str. 89, 14482 Potsdam, Germany). Many thanks to Christian Hammer for supervision of Moritz Kreuzer's master's thesis “Coupling the Ice-Sheet Model PISM to the Climate Model POEM”, which laid the foundation for this publication.

Finally, we appreciate the helpful suggestions and comments from the anonymous reviewer, Rupert Gladstone and Steven Phipps, which led to considerable improvements of the paper.

*Financial support.* This research has been supported by the Deutsche Forschungsgemeinschaft (DFG; grant nos. WI4556/4-1, WI4556/3-1, and WI4556/2-1), the Horizon 2020 programme (grant no. TiPACCs 820575), the German Federal Ministry of Education and Research (BMBF, FONA; grant nos. FKZ:01LP1925D, FKZ:01LP1504D, and FKZ:01LP1502C), NASA (grant no. NNX17AG65G), NSF (grant nos. PLR-1603799 and PLR-1644277), the European Regional Development Fund (ERDF), the German Federal Ministry of Education and Research (BMBF), and the Land Brandenburg.

The publication of this article was funded by the Open Access Fund of the Leibniz Association.

*Review statement.* This paper was edited by Steven Phipps and reviewed by Rupert Gladstone and one anonymous referee.

## References

- Albrecht, T., Winkelmann, R., and Levermann, A.: Glacial-cycle simulations of the Antarctic Ice Sheet with the Parallel Ice Sheet Model (PISM) – Part 1: Boundary conditions and climatic forcing, *The Cryosphere*, 14, 599–632, <https://doi.org/10.5194/tc-14-599-2020>, 2020.
- Asay-Davis, X. S., Jourdain, N. C., and Nakayama, Y.: Developments in Simulating and Parameterizing Interactions Between the Southern Ocean and the Antarctic Ice Sheet, *Curr. Clim. Change Rep.*, 3, 316–329, <https://doi.org/10.1007/s40641-017-0071-0>, 2017.
- Aschwanden, A., Bueler, E., Khrulev, C., and Blatter, H.: An enthalpy formulation for glaciers and ice sheets, *J. Glaciol.*, 58, 441–457, <https://doi.org/10.3189/2012jog11j088>, 2012.
- Balaji, V., Maisonnave, E., Zadeh, N., Lawrence, B. N., Biercamp, J., Fladrich, U., Aloisio, G., Benson, R., Caubel, A., Durachta, J., Foujols, M.-A., Lister, G., Mocavero, S., Underwood, S., and Wright, G.: CPMIP: measurements of real computational performance of Earth system models in CMIP6, *Geosci. Model Dev.*, 10, 19–34, <https://doi.org/10.5194/gmd-10-19-2017>, 2017.
- Beckmann, A. and Goosse, H.: A parameterization of ice shelf-ocean interaction for climate models, *Ocean Model.*, 5, 157–170, [https://doi.org/10.1016/S1463-5003\(02\)00019-7](https://doi.org/10.1016/S1463-5003(02)00019-7), 2003.

- Bronslaer, B., Winton, M., Griffies, S. M., Hurlin, W. J., Rodgers, K. B., Sergienko, O. V., Stouffer, R. J., and Russell, J. L.: Change in future climate due to Antarctic meltwater, *Nature*, 564, 53–58, <https://doi.org/10.1038/s41586-018-0712-z>, 2018.
- Bueler, E. and Brown, J.: Shallow shelf approximation as a “sliding law” in a thermomechanically coupled ice sheet model, *J. Geophys. Res.-Earth Surf.*, 114, F03008, <https://doi.org/10.1029/2008JF001179>, 2009.
- Bueler, E. and van Pelt, W.: Mass-conserving subglacial hydrology in the Parallel Ice Sheet Model version 0.6, *Geosci. Model Dev.*, 8, 1613–1635, <https://doi.org/10.5194/gmd-8-1613-2015>, 2015.
- Bueler, E., Brown, J., and Lingle, C.: Exact solutions to the thermomechanically coupled shallow-ice approximation: effective tools for verification, *J. Glaciol.*, 53, 499–516, <https://doi.org/10.3189/002214307783258396>, 2007.
- Clark, P. U. and Mix, A. C.: Ice sheets and sea level of the Last Glacial Maximum, *Quatern. Sci. Rev.*, 21, 1–7, [https://doi.org/10.1016/S0277-3791\(01\)00118-4](https://doi.org/10.1016/S0277-3791(01)00118-4), 2002.
- Depoorter, M. A., Bamber, J. L., Griggs, J. A., Lenaerts, J. T. M., Ligtenberg, S. R. M., van den Broeke, M. R., and Moholdt, G.: Calving fluxes and basal melt rates of Antarctic ice shelves, *Nature*, 502, 89–92, <https://doi.org/10.1038/nature12567>, 2013.
- De Rydt, J. and Gudmundsson, G. H.: Coupled ice shelf-ocean modeling and complex grounding line retreat from a seabed ridge, *J. Geophys. Res.-Earth Surf.*, 121, 865–880, <https://doi.org/10.1002/2015JF003791>, 2016.
- Dinniman, M., Asay-Davis, X., Galton-Fenzi, B., Holland, P., Jenkins, A., and Timmermann, R.: Modeling Ice Shelf/Ocean Interaction in Antarctica: A Review, *Oceanography*, 29, 144–153, <https://doi.org/10.5670/oceanog.2016.106>, 2016.
- Donat-Magnin, M., Jourdain, N. C., Spence, P., Le Sommer, J., Gallée, H., and Durand, G.: Ice-Shelf Melt Response to Changing Winds and Glacier Dynamics in the Amundsen Sea Sector, Antarctica, *J. Geophys. Res.-Oceans*, 122, 10206–10224, <https://doi.org/10.1002/2017JC013059>, 2017.
- Eyring, V., Bony, S., Meehl, G. A., Senior, C. A., Stevens, B., Stouffer, R. J., and Taylor, K. E.: Overview of the Coupled Model Intercomparison Project Phase 6 (CMIP6) experimental design and organization, *Geosci. Model Dev.*, 9, 1937–1958, <https://doi.org/10.5194/gmd-9-1937-2016>, 2016.
- Favier, L., Jourdain, N. C., Jenkins, A., Merino, N., Durand, G., Gagliardini, O., Gillet-Chaulet, F., and Mathiot, P.: Assessment of sub-shelf melting parameterisations using the ocean-ice-sheet coupled model NEMO(v3.6)–Elmer/Ice(v8.3), *Geosci. Model Dev.*, 12, 2255–2283, <https://doi.org/10.5194/gmd-12-2255-2019>, 2019.
- Feldmann, J., Albrecht, T., Khroulev, C., Pattyn, F., and Levermann, A.: Resolution-dependent performance of grounding line motion in a shallow model compared with a full-Stokes model according to the MISIP3d intercomparison, *J. Glaciol.*, 60, 353–360, <https://doi.org/10.3189/2014JG13J093>, 2014.
- Fretwell, P., Pritchard, H. D., Vaughan, D. G., Bamber, J. L., Barand, N. E., Bell, R., Bianchi, C., Bingham, R. G., Blankenship, D. D., Casassa, G., Catania, G., Callens, D., Conway, H., Cook, A. J., Corr, H. F. J., Damaske, D., Damm, V., Ferraccioli, F., Forsberg, R., Fujita, S., Gim, Y., Gogineni, P., Griggs, J. A., Hindmarsh, R. C. A., Holmlund, P., Holt, J. W., Jacobel, R. W., Jenkins, A., Jokat, W., Jordan, T., King, E. C., Kohler, J., Krabill, W., Riger-Kusk, M., Langley, K. A., Leitchenkov, G., Leuschen, C., Luyendyk, B. P., Matsuoka, K., Mouginot, J., Nitsche, F. O., Nogi, Y., Nost, O. A., Popov, S. V., Rignot, E., Rippon, D. M., Rivera, A., Roberts, J., Ross, N., Siegert, M. J., Smith, A. M., Steinhage, D., Studinger, M., Sun, B., Tinto, B. K., Welch, B. C., Wilson, D., Young, D. A., Xiangbin, C., and Zirizzotti, A.: Bedmap2: improved ice bed, surface and thickness datasets for Antarctica, *The Cryosphere*, 7, 375–393, <https://doi.org/10.5194/tc-7-375-2013>, 2013.
- Galbraith, E. D., Kwon, E. Y., Gnanadesikan, A., Rodgers, K. B., Griffies, S. M., Bianchi, D., Sarmiento, J. L., Dunne, J. P., Simeon, J., Slater, R. D., Wittenberg, A. T., and Held, I. M.: Climate Variability and Radiocarbon in the CM2Mc Earth System Model, *J. Climate*, 24, 4230–4254, <https://doi.org/10.1175/2011JCLI3919.1>, 2011.
- Garabato, A. C. N., Forryan, A., Dutrieux, P., Brannigan, L., Biddle, L. C., Heywood, K. J., Jenkins, A., Firing, Y. L., and Kimura, S.: Vigorous lateral export of the meltwater outflow from beneath an Antarctic ice shelf, *Nature*, 542, 219–222, <https://doi.org/10.1038/nature20825>, 2017.
- Gladstone, R., Galton-Fenzi, B., Gwyther, D., Zhou, Q., Hattermann, T., Zhao, C., Jong, L., Xia, Y., Guo, X., Petrakopoulos, K., Zwinger, T., Shapero, D., and Moore, J.: The Framework For Ice Sheet–Ocean Coupling (FISOC) V1.1, *Geosci. Model Dev.*, 14, 889–905, <https://doi.org/10.5194/gmd-14-889-2021>, 2021.
- Goelzer, H., Huybrechts, P., Loutre, M.-F., and Fichefet, T.: Last Interglacial climate and sea-level evolution from a coupled ice sheet–climate model, *Clim. Past*, 12, 2195–2213, <https://doi.org/10.5194/cp-12-2195-2016>, 2016.
- Golledge, N., Keller, E., Gomez, N., Naughten, K., Bernales, J., Trusel, L., and Edwards, T.: Global environmental consequences of twenty-first-century ice-sheet melt, *Nature*, 566, 65–72, <https://doi.org/10.1038/s41586-019-0889-9>, 2019.
- Griffies, S. M.: Elements of the Modular Ocean Model (MOM), Tech. Rep. GFDL Ocean Group Technical Report No. 7, NOAA/Geophysical Fluid Dynamics Laboratory, available at: [https://mom-ocean.github.io/assets/pdfs/MOM5\\_manual.pdf](https://mom-ocean.github.io/assets/pdfs/MOM5_manual.pdf) (last access: 15 June 2021), 2012.
- Griffies, S. M., Biastoch, A., Böning, C., Bryan, F., Danabasoglu, G., Chassignet, E. P., England, M. H., Gerdes, R., Haak, H., Hallberg, R. W., Hazeleger, W., Jungclaus, J., Large, W. G., Madec, G., Pirani, A., Samuels, B. L., Scheinert, M., Gupta, A. S., Severijns, C. A., Simmons, H. L., Treguier, A. M., Winton, M., Yeager, S., and Yin, J.: Coordinated Ocean-ice Reference Experiments (COREs), *Ocean Model.*, 26, 1–46, <https://doi.org/10.1016/j.ocemod.2008.08.007>, 2009.
- Heuzé, C., Heywood, K. J., Stevens, D. P., and Ridley, J. K.: Southern Ocean bottom water characteristics in CMIP5 models, *Geophys. Res. Lett.*, 40, 1409–1414, <https://doi.org/10.1002/grl.50287>, 2013.
- Hillenbrand, C.-D., Smith, J. A., Hodell, D. A., Greaves, M., Poole, C. R., Kender, S., Williams, M., Andersen, T. J., Jernas, P. E., Elderfield, H., Klages, J. P., Roberts, S. J., Gohl, K., Larter, R. D., and Kuhn, G.: West Antarctic Ice Sheet retreat driven by Holocene warm water incursions, *Nature*, 547, 43–48, <https://doi.org/10.1038/nature22995>, 2017.
- Holland, D. M. and Jenkins, A.: Modeling Thermodynamic Ice–Ocean Interactions at the Base of an Ice Shelf, *J. Phys. Oceanogr.*, 29, 1787–1800, [https://doi.org/10.1175/1520-0485\(1999\)029<1787:mtioia>2.0.co;2](https://doi.org/10.1175/1520-0485(1999)029<1787:mtioia>2.0.co;2), 1999.

- Holland, P. R., Bracegirdle, T. J., Dutrieux, P., Jenkins, A., and Steig, E. J.: West Antarctic ice loss influenced by internal climate variability and anthropogenic forcing, *Nat. Geosci.*, 12, 718–724, <https://doi.org/10.1038/s41561-019-0420-9>, 2019.
- Jenkins, A., Shoosmith, D., Dutrieux, P., Jacobs, S., Kim, T. W., Lee, S. H., Ha, H. K., and Stammerjohn, S.: West Antarctic Ice Sheet retreat in the Amundsen Sea driven by decadal oceanic variability, *Nat. Geosci.*, 11, 733–738, <https://doi.org/10.1038/s41561-018-0207-4>, 2018.
- Jordan, J. R., Holland, P. R., Goldberg, D., Snow, K., Arthern, R., Campin, J.-M., Heimbach, P., and Jenkins, A.: Ocean-Forced Ice-Shelf Thinning in a Synchronously Coupled Ice-Ocean Model, *J. Geophys. Res.-Oceans*, 123, 864–882, <https://doi.org/10.1002/2017jc013251>, 2018.
- Jourdain, N. C., Asay-Davis, X., Hattermann, T., Straneo, F., Seroussi, H., Little, C. M., and Nowicki, S.: A protocol for calculating basal melt rates in the ISMIP6 Antarctic ice sheet projections, *The Cryosphere*, 14, 3111–3134, <https://doi.org/10.5194/tc-14-3111-2020>, 2020.
- Khrulev, C., Bueller, E., Aschwanden, A., Maxwell, D., Brown, J., Albrecht, T., Seguinot, J., Mengel, M., Hinck, S., Kreuzer, M., Ziemer, F., Reese, R., and Kleiner, T.: m-kreuzer/pism: Version as used in Kreuzer et al., Geoscientific Model Development publication (gmd-2020-230) (Version v1.1.4\_gmd-2020-230), Zenodo, <https://doi.org/10.5281/zenodo.4686967>, 2021.
- Kreuzer, M.: m-kreuzer/PISM-MOM\_coupling: Version as used in Kreuzer et al., Geoscientific Model Development publication (gmd-2020-230) (Version v1.0.3), Zenodo, <https://doi.org/10.5281/zenodo.4692679>, 2021a.
- Kreuzer, M.: Input Data as used in Kreuzer et al., Geoscientific Model Development publication (gmd-2020-230) (Version v1.0.3) [Data set], Zenodo, <https://doi.org/10.5281/zenodo.4692940>, 2021b.
- Leslie, T., Ward, M., Hannah, N., Hoover, N., Heerdegen, A., Griffies, S., Kiss, A., Fiedler, R., Holmes, R., Yan, H., Farneti, R., Leopardi, P., Snow, K., Castelão, G., Underwood, S., naught101, and Liang, Z.: m-kreuzer/MOM5: Version as used in Kreuzer et al., Geoscientific Model Development publication (gmd-2020-230) (Version 5.1.0\_gmd-2020-230), Zenodo, <https://doi.org/10.5281/zenodo.3991665>, 2020.
- Levermann, A., Albrecht, T., Winkelmann, R., Martin, M. A., Haseloff, M., and Joughin, I.: Kinematic first-order calving law implies potential for abrupt ice-shelf retreat, *The Cryosphere*, 6, 273–286, <https://doi.org/10.5194/tc-6-273-2012>, 2012.
- Lewis, E. L. and Perkin, R. G.: Ice pumps and their rates, *J. Geophys. Res.-Oceans*, 91, 11756–11762, <https://doi.org/10.1029/JC091iC10p11756>, 1986.
- Lowry, D. P., Golledge, N. R., Bertler, N. A. N., Jones, R. S., and McKay, R.: Deglacial grounding-line retreat in the Ross Embayment, Antarctica, controlled by ocean and atmosphere forcing, *Sci. Adv.*, 5, eaav8754, <https://doi.org/10.1126/sciadv.aav8754>, 2019.
- MacAyeal, D. R.: Large-scale ice flow over a viscous basal sediment: Theory and application to ice stream B, Antarctica, *J. Geophys. Res.-Sol. Ea.*, 94, 4071–4087, <https://doi.org/10.1029/JB094iB04p04071>, 1989.
- Martin, T. and Adcroft, A.: Parameterizing the fresh-water flux from land ice to ocean with interactive icebergs in a coupled climate model, *Ocean Model.*, 34, 111–124, <https://doi.org/10.1016/j.ocemod.2010.05.001>, 2010.
- Mouginot, J., Scheuchl, B., and Rignot, E.: Mapping of Ice Motion in Antarctica Using Synthetic-Aperture Radar Data, *Remote Sens.*, 4, 2753–2767, <https://doi.org/10.3390/rs4092753>, 2012.
- Murray, R. J.: Explicit Generation of Orthogonal Grids for Ocean Models, *J. Comput. Phys.*, 126, 251–273, <https://doi.org/10.1006/jcph.1996.0136>, 1996.
- Nakayama, Y., Menemenlis, D., Zhang, H., Schodlok, M., and Rignot, E.: Origin of Circumpolar Deep Water intruding onto the Amundsen and Bellingshausen Sea continental shelves, *Nat. Commun.*, 9, 3403, <https://doi.org/10.1038/s41467-018-05813-1>, 2018.
- Naughten, K. A., Rydt, J. D., Rosier, S. H. R., Jenkins, A., Holland, P. R., and Ridley, J. K.: Two-timescale response of a large Antarctic ice shelf to climate change, *Nat. Commun.*, 12, 1991, <https://doi.org/10.1038/s41467-021-22259-0>, 2021.
- Nowicki, S., Goelzer, H., Seroussi, H., Payne, A. J., Lipscomb, W. H., Abe-Ouchi, A., Agosta, C., Alexander, P., Asay-Davis, X. S., Barthel, A., Bracegirdle, T. J., Cullather, R., Felikson, D., Fettweis, X., Gregory, J. M., Hattermann, T., Jourdain, N. C., Kuipers Munneke, P., Larour, E., Little, C. M., Morlighem, M., Nias, I., Shepherd, A., Simon, E., Slater, D., Smith, R. S., Straneo, F., Trusel, L. D., van den Broeke, M. R., and van de Wal, R.: Experimental protocol for sea level projections from ISMIP6 stand-alone ice sheet models, *The Cryosphere*, 14, 2331–2368, <https://doi.org/10.5194/tc-14-2331-2020>, 2020.
- Olbers, D. and Hellmer, H.: A box model of circulation and melting in ice shelf caverns, *Ocean Dynam.*, 60, 141–153, <https://doi.org/10.1007/s10236-009-0252-z>, 2010.
- Pauling, A. G., Bitz, C. M., Smith, I. J., and Langhorne, P. J.: The Response of the Southern Ocean and Antarctic Sea Ice to Freshwater from Ice Shelves in an Earth System Model, *J. Climate*, 29, 1655–1672, <https://doi.org/10.1175/JCLI-D-15-0501.1>, 2016.
- Reese, R., Albrecht, T., Mengel, M., Asay-Davis, X., and Winkelmann, R.: Antarctic sub-shelf melt rates via PICO, *The Cryosphere*, 12, 1969–1985, <https://doi.org/10.5194/tc-12-1969-2018>, 2018.
- Reese, R., Levermann, A., Albrecht, T., Seroussi, H., and Winkelmann, R.: The role of history and strength of the oceanic forcing in sea level projections from Antarctica with the Parallel Ice Sheet Model, *The Cryosphere*, 14, 3097–3110, <https://doi.org/10.5194/tc-14-3097-2020>, 2020.
- Rignot, E., Mouginot, J., and Scheuchl, B.: Ice Flow of the Antarctic Ice Sheet, *Science*, 333, 1427–1430, <https://doi.org/10.1126/science.1208336>, 2011.
- Rignot, E., Jacobs, S., Mouginot, J., and Scheuchl, B.: Ice-Shelf Melting Around Antarctica, *Science*, 341, 266–270, <https://doi.org/10.1126/science.1235798>, 2013.
- Rignot, E., Mouginot, J., and Scheuchl, B.: MEaSUREs InSAR-Based Antarctica Ice Velocity Map, Version 2, National Snow & Ice Data Center (NSIDC), <https://doi.org/10.5067/D7GK8F5J8M8R>, 2017.
- Schmidtke, S., Heywood, K. J., Thompson, A. F., and Aoki, S.: Multidecadal warming of Antarctic waters, *Science*, 346, 1227–1231, <https://doi.org/10.1126/science.1256117>, 2014.
- Schulzweida, U.: CDO User Guide (Version 1.9.6), Manual, MPI for Meteorology Hamburg, available at: <https://doi.org/10.5194/gmd-14-3697-2021>

- //code.mpimet.mpg.de/projects/cdo/embedded/cdo.pdf (last access: 16 April 2021), 2019.
- Schulzweida, U., Mueller, R., Heidmann, O., Ansorge, C., Kornblueh, L., Wachsmann, F., Kameswarrao, M., and Quast, R.: Climate Data Operator (CDO) (Version 1.9.6), Zenodo, <https://doi.org/10.5281/zenodo.3991595>, 2019.
- Seroussi, H., Nakayama, Y., Larour, E., Menemenlis, D., Morlighem, M., Rignot, E., and Khazendar, A.: Continued retreat of Thwaites Glacier, West Antarctica, controlled by bed topography and ocean circulation, *Geophys. Res. Lett.*, 44, 6191–6199, <https://doi.org/10.1002/2017GL072910>, 2017.
- Seroussi, H., Nowicki, S., Payne, A. J., Goelzer, H., Lipscomb, W. H., Abe-Ouchi, A., Agosta, C., Albrecht, T., Asay-Davis, X., Barthel, A., Calov, R., Cullather, R., Dumas, C., Galton-Fenzi, B. K., Gladstone, R., Golledge, N. R., Gregory, J. M., Greve, R., Hattermann, T., Hoffman, M. J., Humbert, A., Huybrechts, P., Jourdain, N. C., Kleiner, T., Larour, E., Leguy, G. R., Lowry, D. P., Little, C. M., Morlighem, M., Pattyn, F., Pelle, T., Price, S. F., Quiquet, A., Reese, R., Schlegel, N.-J., Shepherd, A., Simon, E., Smith, R. S., Straneo, F., Sun, S., Trusel, L. D., Van Breedam, J., van de Wal, R. S. W., Winkelmann, R., Zhao, C., Zhang, T., and Zwinger, T.: ISMIP6 Antarctica: a multi-model ensemble of the Antarctic ice sheet evolution over the 21st century, *The Cryosphere*, 14, 3033–3070, <https://doi.org/10.5194/tc-14-3033-2020>, 2020.
- Shapiro, N. M. and Ritzwoller, M. H.: Inferring surface heat flux distributions guided by a global seismic model: particular application to Antarctica, *Earth Planet. Sc. Lett.*, 223, 213–224, <https://doi.org/10.1016/j.epsl.2004.04.011>, 2004.
- Shepherd, A., Ivins, E., Rignot, E., Smith, B., Van den Broeke, M., Whitehouse, P., Briggs, K., Joughin, I., Krinner, G., Nowicki, S., Payne, A., Scambos, T., Schlegel, N., Aa, G., Agosta, C., Ahlstrøm, A., Babonis, G., Barletta, V., Blazquez, A., and Wouters, B.: Mass balance of the Antarctic Ice Sheet from 1992 to 2017, *Nature*, 558, 219–222, <https://doi.org/10.1038/s41586-018-0179-y>, 2018.
- Slater, J. A. and Malys, S.: WGS 84 – Past, Present and Future, in: *Advances in Positioning and Reference Frames*, Springer Berlin Heidelberg, 1–7, [https://doi.org/10.1007/978-3-662-03714-0\\_1](https://doi.org/10.1007/978-3-662-03714-0_1), 1998.
- Stern, A. A., Adcroft, A., and Sergienko, O.: The effects of Antarctic iceberg calving-size distribution in a global climate model, *J. Geophys. Res.-Oceans*, 121, 5773–5788, <https://doi.org/10.1002/2016jc011835>, 2016.
- Taylor, K. E., Stouffer, R. J., and Meehl, G. A.: An Overview of CMIP5 and the Experiment Design, *B. Am. Meteorol. Soc.*, 93, 485–498, <https://doi.org/10.1175/BAMS-D-11-00094.1>, 2012.
- Timmermann, R. and Goeller, S.: Response to Filchner–Ronne Ice Shelf cavity warming in a coupled ocean–ice sheet model – Part 1: The ocean perspective, *Ocean Sci.*, 13, 765–776, <https://doi.org/10.5194/os-13-765-2017>, 2017.
- Tournadre, J., Bouhier, N., Girard-Ardhuin, F., and Rémy, F.: Antarctic icebergs distributions 1992–2014, *J. Geophys. Res.-Oceans*, 121, 327–349, <https://doi.org/10.1002/2015jc011178>, 2016.
- van Wessem, J. M., van de Berg, W. J., Noël, B. P. Y., van Meijgaard, E., Amory, C., Birnbaum, G., Jakobs, C. L., Krüger, K., Lenaerts, J. T. M., Lhermitte, S., Ligtenberg, S. R. M., Medley, B., Reijmer, C. H., van Tricht, K., Trusel, L. D., van Ulf, L. H., Wouters, B., Wuite, J., and van den Broeke, M. R.: Modelling the climate and surface mass balance of polar ice sheets using RACMO2 – Part 2: Antarctica (1979–2016), *The Cryosphere*, 12, 1479–1498, <https://doi.org/10.5194/tc-12-1479-2018>, 2018.
- Vizcaíno, M., Lipscomb, W. H., Sacks, W. J., and van den Broeke, M.: Greenland Surface Mass Balance as Simulated by the Community Earth System Model. Part II: Twenty-First-Century Changes, *J. Climate*, 27, 215–226, <https://doi.org/10.1175/JCLI-D-12-00588.1>, 2014.
- Winkelmann, R., Martin, M. A., Haseloff, M., Albrecht, T., Bueler, E., Khroulev, C., and Levermann, A.: The Potsdam Parallel Ice Sheet Model (PISM-PIK) – Part 1: Model description, *The Cryosphere*, 5, 715–726, <https://doi.org/10.5194/tc-5-715-2011>, 2011.
- Winton, M.: A Reformulated Three-Layer Sea Ice Model, *J. Atmos. Ocean. Tech.*, 17, 525–531, [https://doi.org/10.1175/1520-0426\(2000\)017<0525:ARTLSI>2.0.CO;2](https://doi.org/10.1175/1520-0426(2000)017<0525:ARTLSI>2.0.CO;2), 2000.
- Zender, C. S.: netCDF Operator (NCO) User Guide (Version 4.7.8), Manual, available at: <http://nco.sf.net/nco.pdf> (last access: 16 April 2021), 2018.
- Zender, C., Vicente, P., hmb1, Wang, D. L., wenshanw, Mao, J., dywei, Fernando, I., Filipe, Couwenberg, B., Neumann, D., jedwards4b, Hegewald, J., Hamman, J., and Oliveira, H.: nco/nco: Paradise Lost (Version 4.7.8), Zenodo, <https://doi.org/10.5281/zenodo.1490166>, 2018.
- Ziemen, F. A., Kapsch, M.-L., Klockmann, M., and Mikolajewicz, U.: Heinrich events show two-stage climate response in transient glacial simulations, *Clim. Past*, 15, 153–168, <https://doi.org/10.5194/cp-15-153-2019>, 2019.
- Zwally, H. J., Giovinetto, M. B., Beckley, M. A., and Saba, J. L.: Antarctic and Greenland Drainage Systems, available at: [http://icesat4.gsfc.nasa.gov/cryo\\_data/ant\\_grn\\_drainage\\_systems.php](http://icesat4.gsfc.nasa.gov/cryo_data/ant_grn_drainage_systems.php) (last access: 16 April 2021), 2012.